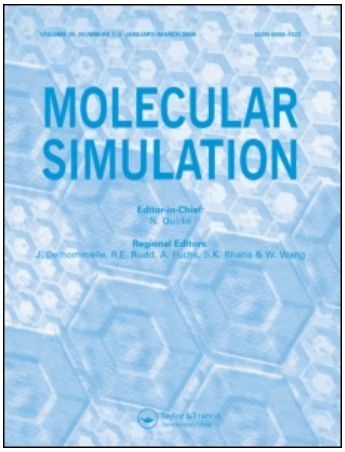

Molecular Simulation
Publication details, including instructions for authors and subscription information:
http://www.informaworld.com/smpp/title~content=t713644482

Molecular dynamics simulation of formation and control of nanodroplets in piezoelectric nanoejection systems

Chi-Fu Dai[a]; Rong-Yeu Chang[a]
[a] Department of Chemical Engineering, National Tsing-Hua University, Hsinchu, Taiwan, R.O.C.

Online publication date: 15 October 2010

To cite this Article Dai, Chi-Fu and Chang, Rong-Yeu(2010) 'Molecular dynamics simulation of formation and control of nanodroplets in piezoelectric nanoejection systems', Molecular Simulation, 36: 11, 847 — 855
To link to this Article: DOI: 10.1080/08927022.2010.484022
URL: http://dx.doi.org/10.1080/08927022.2010.484022

Molecular Simulation
Vol. 36, No. 11, September 2010, 847–855

Taylor & Francis
Taylor & Francis Group

Molecular dynamics simulation of formation and control of nanodroplets in piezoelectric nanoejection systems

Chi-Fu Dai* and Rong-Yeu Chang

Department of Chemical Engineering, National Tsing-Hua University, P.O. Box 30043, Hsinchu, Taiwan, R.O.C.

(*Received 27 August 2009; final version received 6 April 2010*)

In this paper, the formation of nanodroplets in piezoelectric nanoejection processes is investigated by non-equilibrium molecular dynamics simulation. By compressing liquid propane molecules with various specific pushing periods of oscillation, the phenomena of liquid thread breakup and droplet formation are simulated. The simulation results revealed that various features aid the piezoelectric nanoejection system. Two breakup shapes including double-cone and long tail structures were found in this process. To analyse the ejection process in detail, 2D contour plots and thermal properties for various pushing periods are shown and discussed in this paper. The results show that the sizes of nanodroplets are linear depending on the pushing periods. The findings show a new control factor and mechanism for nanodroplet formation through piezoelectric nanoejection processes.

Keywords: simulation; molecular dynamics; nanojet ejection

1. Introduction

Piezoelectric ejection [1] is a type of drop-on-demand (DOD) inkjet printing technology. A DOD device will only create and eject droplets to the specific surface where droplets are needed. Piezoelectric inkjet print heads offer several advantages such as high-print quality, high-chemical resistance, long life and low limitation of ink selection. Recently, with the progress of nanomachining [2,3], nanosized nozzles have been developed. Naik et al. [3] reported on microfluidics for the generation and characterisation of liquid and gaseous micro- and nanojets. Piezoelectric inkjet printing has been applied to other industrial process technologies; piezoelectric inkjet printer not only solves the problems that occur in large-area fabrication processes, but also effectively lowers the cost of fabrication, enhances competitiveness or creates a new industry, thereby paving the way for a considerable number of industrial applications at both macro- and nanoscales [4]. It is accepted that continuum mechanics is good at describing the nonlinear dynamics, free-surface jet flow [5] and viscoelastic fluid jet [6] at the macroscale. However, jet breakup and the spray model require assumptions or experiential correlations, which are difficult to find for the nanojet process. Therefore, the continuum model is not applicable when nanoscale or molecular-level physics is dominant. Non-equilibrium molecular dynamics (MD) simulation is a powerful tool used to predict the processes under various conditions in a nanoscale environment.

Recently, many researchers have reported MD simulation results [7–14] and have presented theory [15] regarding nanojet formation. Moseler and Landman [7] first presented MD simulation results for a molecular propane fluid jet system with a gold nozzle of diameter 6 nm. They also suggested a stochastic hydrodynamic lubrication equation (SLE) [7,8] based on Navier–Stokes equations with a Gaussian white-noise distribution to describe the jet profile evolution. Shin et al. [9] observed that the droplet sizes and jet breakup characteristics in an argon nanojet injection still resemble the Rayleigh breakup theory. Choi et al. [10] reported the ejection behaviour of a nanojet with nozzles of varying diameters; the results showed the effect of nozzle outlet size on the breakup time and on the growth rate of spherical droplets. Ichiki and Consta [11] reported the formation of charged nanodroplets by MD simulation and analytical models. Murad and Puri [12] reported on nanoscale jet collisions for various impact velocities and found that the duration between collision and recoil is dependent on impact velocity. Shin et al. [13] reported on nanojet injection in a high-pressure environment. Kang et al. [14] demonstrated a method for controlling the direction of a liquid propane nanojet through non-uniform asymmetric heating of a nozzle. On the basis of MD simulation results [7], Eggers [15] used self-similar profiles to describe the breakup mode and dynamics of liquid nanojets. Tiwari and Abraham [16] simulated a liquid nanojet breakup in a dissipative particle dynamics (DPD) two-phase model. They observed that the breakup of nanojets is accelerated by thermal fluctuations. They also showed that the DPD

*Corresponding author. Email: cfdai@che.nthu.edu.tw

ISSN 0892-7022 print/ISSN 1029-0435 online

DOI: 10.1080/08927022.2010.484022
http://www.informaworld.com

two-phase model offers results similar to those obtained from MD simulations [9].

These previous studies prove that nanojet flow methods are a promising research topic in technological applications and scientific investigations. Some characteristics of nanojets and of the formation of nanodroplets have been mentioned in these studies. However, the ejection systems that are presented in the previous studies are modelled with constant velocity or constant pressure; the droplet size and number cannot be accurately controlled. Thus, this research built up a piezoelectric nanoejection simulation system with specific pushing periods of oscillation to investigate the piezoelectric ejection process at nanoscale. The realisation of a piezoelectric nanoejection process will be useful in assisting future design and motivate us to explore its use in nanoscale manufacturing processes. In this paper, the formation of nanodroplets and the breakup behaviour in piezoelectric nanoejection processes are investigated by non-equilibrium MD simulation.

2. Simulation method and system

2.1 Simulation modelling and parameters

In this paper, non-equilibrium MD simulation is used for providing insights into nanoscale structural features and the dynamics of nanojet flow. Specific potential models are used to describe the interaction between different molecules and atoms. The interaction force can be calculated as the negative derivative of the potential model. In this paper, the shifted Lennard-Jones 12-6 potential [17,18] is used to model the inter-molecular interaction. The shifted Lennard-Jones 12-6 potential is also used to model the interaction between metal wall particles and propane molecules but with different parameters [19]. The united-atom model [20,21] is used to model the propane molecule as three particles. Each particle represents a CH_n ($n = 2, 3$) group unit. Each unit is considered as a mass point having the entire mass of the CH_n group. Therefore, each propane molecule contains three sites: one CH_2 site connected to two CH_3 sites with a spring. The units interact with others by means of inter-molecular interactions and bonded forces. The accuracy of the potential models and the methods used in this study has been confirmed in a previous research [22]. Harmonic potential functions [20] are used for describing the vibrations of liquid propane molecules. The equilibrium values for the carbon–carbon bond length and the C–C–C bond angle are 1.526 Å and 112.4°, respectively. Atoms in the solid walls oscillate from their initial lattice sites. To simulate this thermal fluctuation of metal particles, we employed a nonlinear spring potential model [23]. The simulation models and parameters used in this study are listed in Table 1.

The temperature of the gold nozzle is controlled by the velocity-scaling method [17], which is shown in Equation (1):

$$v_i^{\text{new}} = v_i \sqrt{T_D / T_A}, \tag{1}$$

where T_A represents the actual temperature of the system; T_D, the desired temperature of the system; v_i, the original velocity of the atoms; and v_i^{new}, the modified velocity of the atoms.

Before ejection, the temperature of the fluid molecules is controlled by the Nosé–Hoover [24] thermostat, which is shown in Equation (2):

$$\begin{gathered} v_i = P_i / m_i, \quad \dot{P}_i = F - \zeta \cdot P_i, \\ Q\zeta = \sum_i P_i / m_i - gkT_D, \end{gathered} \tag{2}$$

where P_i represents the momentum of the atoms; $\dot{P}_i$, the acceleration; and m_i, the mass. ζ and Q are the method parameters.

The equation of motion is integrated by the fifth-order Gear predictor–corrector method [17]. The integral time interval in this research is about 1 fs.

2.2 Simulation system

The geometry of the simulation system is illustrated in Figure 1. The entire piezoelectric ejection process is

Table 1. Intermolecular potential models and parameters used in this study.

Particle groups	Potential model	Parameters	
Fluid particles (CH_3, CH_2)	$U_s(r) = \begin{cases} U_{LJ}(r) - U_{LJ}(r_c) - [r - r_c]\left(\frac{dU_{LJ}}{dr}\right)_{r_c} & r \le r_c \\ 0 & r > r_c \end{cases}$	$\sigma_{CH_3-CH_3} = 0.387$ (nm) $\sigma_{CH_2-CH_2} = 0.387$ (nm) $\varepsilon_{CH_3-CH_3} = 88.06$ (K) $\varepsilon_{CH_2-CH_2} = 59.38$ (K)	[20]
Wall particles (Au)	$U_{LJ} = 4\varepsilon\left[\left(\frac{\sigma}{r_{ij}}\right)^{12} - \left(\frac{\sigma}{r_{ij}}\right)^{6}\right]$	$\sigma_{Au-CH_2CH_3} = 0.3271$ (nm) $\varepsilon_{Au-CH_2CH_3} = 215.81$ (K)	[19]
Wall particles	$U_{\text{nonlinear}} = \frac{H_1}{2}R^2 + \frac{H_2}{4d_{er}^2}R^4 + \frac{H_3}{6d_{er}^4}R^6$	$H_1 = 57$, $H_2 = 20$, $H_3 = 50$	[23]

Notes: ε represents the potential energy; σ, the equilibrium distance between two atoms; r_{ij}, the distance between two atoms; and r_c, the cut-off radius (set as 2.5σ in this study to reduce computational time). The parameters for different particle groups, which are obtained from the Lorentz–Berthelot mixing rule [25], are $\sigma_{ij} = (\sigma_{ii} + \sigma_{jj})/2$ and $\varepsilon_{ij} = \sqrt{\varepsilon_{ii}\varepsilon_{jj}}$, H_1,H_2 and H_3 are the parameters of the nonlinear spring potential. R is the displacement of the particle position from the original lattice position. The critical displacement of lattice position d_c is set as 0.0025 times the lattice length.

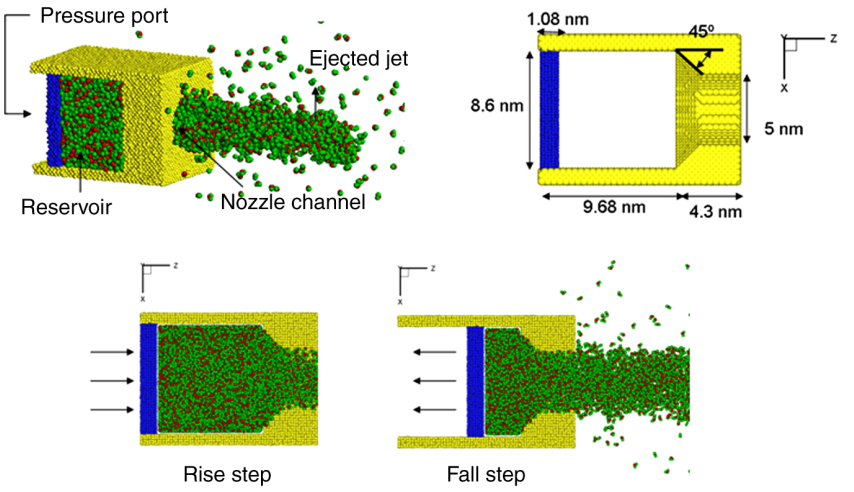

Figure 1. Geometry of the piezoelectric nanojet. CH_3 particles of propane molecules are shown in green; CH_2 particles of propane molecules in red; wall molecules in yellow and the pressure port molecules in blue (colour online).

simulated using a gold nozzle and propane molecules that are a common ejection fluid in MD simulations [7,8,14,22]. The entire nozzle is constructed using an FCC lattice and contains 29,090 Au atoms. The diameter of the nozzle channel is 5 nm. A plate placed behind the reservoir functions as a pressure port and contains 5412 Au atoms. The fluid reservoir initially contains 6000 random propane molecules that are contained in a reservoir of dimensions 8.6 nm × 8.6 nm × 8.98 nm. The pushing period of the piezoelectric ejection process consists of one rise step and one fall step. To simplify the simulation process, we employ only one pushing period in each case. During the rise step, the pushing plate moves forwards towards the outlet of the nozzle, and during the fall step, the pushing plate moves back to its original position. By pushing and pulling the pressure port inside the reservoir, liquid is squeezed out of the nozzle in the form of droplets. In order to avoid any skewing of the results by any non-ideal conditions present during the preparation period, all the simulation results used to obtain average values are collected after the system has reached equilibrium. Subsequent to the initial equilibration of the system at around 150 K, the pushing plate compresses the liquid propane molecules with various specific pushing periods; thus, liquid thread breakup and droplet formation were simulated. The initial temperature for the solid wall and fluid molecules is 150 K, and the temperature of the solid wall is maintained at 150 K throughout the simulation.

In order to determine the specific compressing velocity and pushing periods, the influence of compressing velocity on fluid molecules in nanojet processes was previously investigated [22]. From those results, a specific compressing velocity of 44 m/s was found to offer the most stability and was chosen as the compressing velocity for this study. The first breakup time, 80 ps, was chosen as the unit of pushing periods. The pushing period was varied to investigate the formation of nanodroplets and the formation of the breakup behaviour in piezoelectric nanoejection processes. Based on the first breakup time of the specific compressing velocity [22], three different pushing periods of 80, 160 and 240 ps were set for this study. To avoid the effect of initial condition, three different initial conditions were simulated in each case.

3. Results and discussion

3.1 Ejection process results at various pushing periods

Snapshots of the nanoejection processes at various pushing periods are shown in Figure 2(a)–(c). Figure 2(a) shows a snapshot of the lowest pushing period (80 ps). During the rise step (0–40 ps), the fluid molecules are compressed into the nozzle channel and form a cylindrical liquid thread. The liquid thread maintains propagation through the rise step and fall step. During the fall step (40–80 ps), breakup behaviour can be observed at 70 and 80 ps. Owing to the influence of the balance between surface tension and inertia force, the first breakup occurs at the front end of the liquid thread. The breakup profiles tend to resemble the double-cone structure reported in a related research [7]. Furthermore, another breakup occurs at the mouth of the nozzle at 80 ps; this breakup is caused by the intra-force and the drag force exerted by the plate. As the plate moves back to its original position, the liquid molecules in the reservoir will be dominated by the adsorption force of the plate. Subsequent to the liquid thread breakup, the liquid molecules will recoil into a sphere and result in a nanodroplet with a size similar to that of the first droplet.

Figure 2(b) shows snapshots of the nanojet process at 160 ps pushing periods. The rise step (0–80 ps) is similar to that observed in the previous case, which is shown

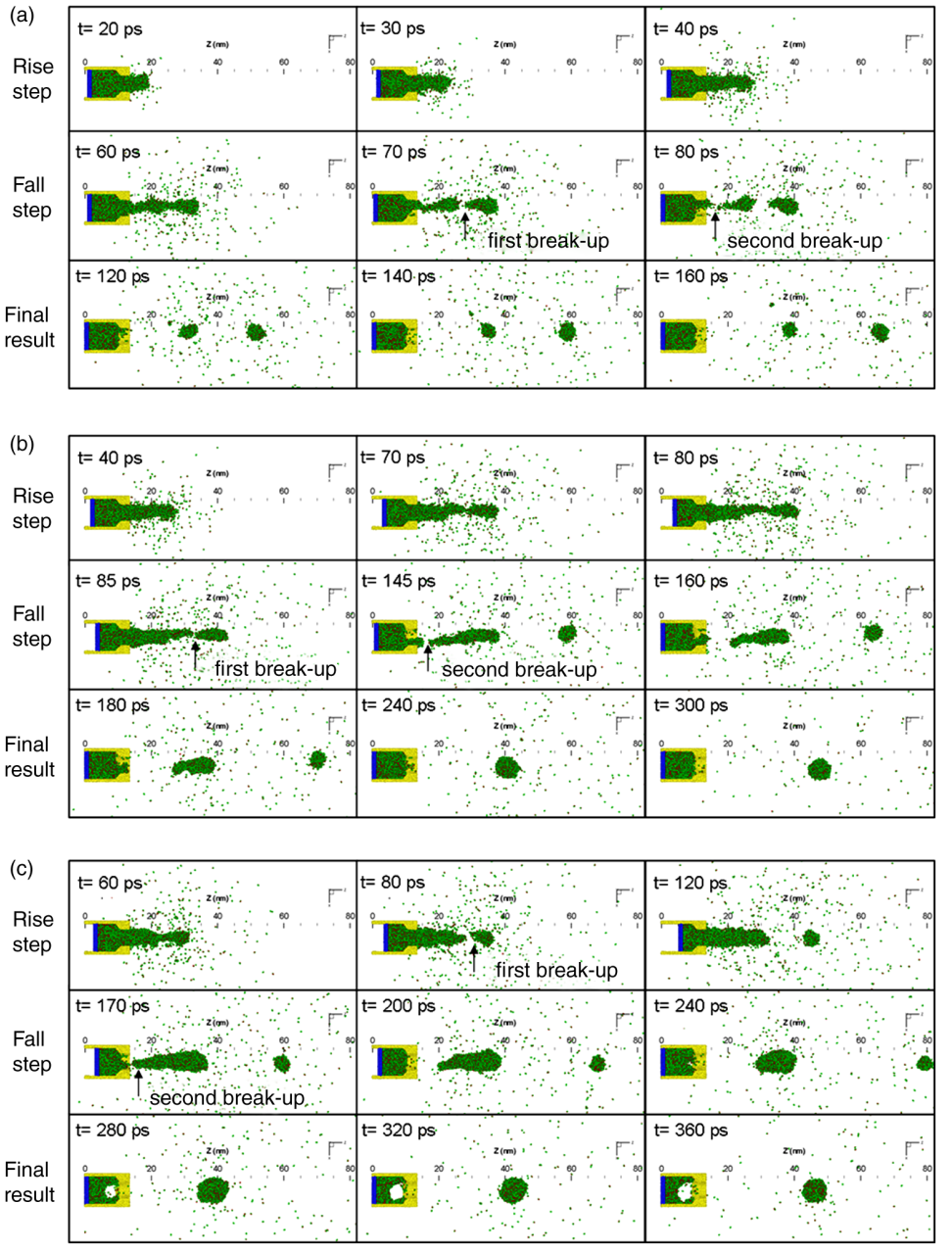

Figure 2. Snapshots of the piezoelectric ejection process with a compressing velocity of 44 m/s. Pushing periods are (a) 80 ps, (b) 160 ps and (c) 240 ps.

in Figure 2(a). During the fall step (80–160 ps), the liquid thread ruptures at the first breakup and then forms the first droplet. The second breakup also occurs at the mouth of the nozzle at 145 ps and then forms a long liquid thread. The liquid thread recoils into a nanodroplet larger than that observed in the previous case (Figure 2(a)). The nanojet process with the longest pushing period (240 ps) is shown in Figure 2(c). It is apparent that the main difference between this case and the other cases is that the profile of the second breakup at 195 ps is a long thread shape that is not similar to the double-cone structure observed in the other cases. This is because the fluid molecules tend to form a longer liquid thread if the rise step is longer. Furthermore, we can observe that a cavity has formed inside the reservoir at 320 ps (Figure 2(c)). This is because of the ejection of a large number of fluid propane molecules from the nozzle. As the pushing periods increase, more fluid molecules are ejected from the nozzle, and the scope of the cavities becomes more obvious.

Thus, two breakups appear in each nanoejection process, and the different breakup structures show that they are formed under different conditions. The first

breakup is a double-cone structure that appears during the forward movement of the thread at similar pushing periods (70–85 ps). This breakup structure is a result of the balance between surface tension and inertia force. The second breakup structure is a long tail structure that appears at the mouth of the nozzle. This structure is a result of stretching of the liquid molecules by the intra-force and the drag force exerted by the plate. Hence, the pushing period influences the formation of the second breakup structure.

3.2 *Two-dimensional property distributions*

Two-dimensional plots of the spatial variations of the nanojet properties for various pushing periods at specific times are shown in Figure 3(a)–(c); these plots are used to analyse the ejection process in detail. The dimensions of each sampling cell are 0.76 nm × 0.76 nm. The layer density distribution (Figure 3(a)) shows that the density is neither uniform nor continuous at nanoscale. Local maximum high-density regions of approximately 0.6 g/cm^3 appeared near the pressure port. The density distributions also show the long thread structure in the breakup location in the cases of long pushing periods. The low-density region appearing in the nozzle outlet shows that the cavity appears after the liquid is ejected. The density of droplets adjusted at a pushing period of 240 ps is about 0.6 g/cm^3, which is higher than that observed in the other cases. This is because the size of the droplet increases in the *y*-axis. A layered density structure can also be found between the vapour–liquid interfaces.

Figure 3(b) shows the pressure distribution. Similar to the density distribution, local high-pressure regions appear near the pressure port. Owing to the fact that a vacuum environment surrounds the nozzle system, the pressure

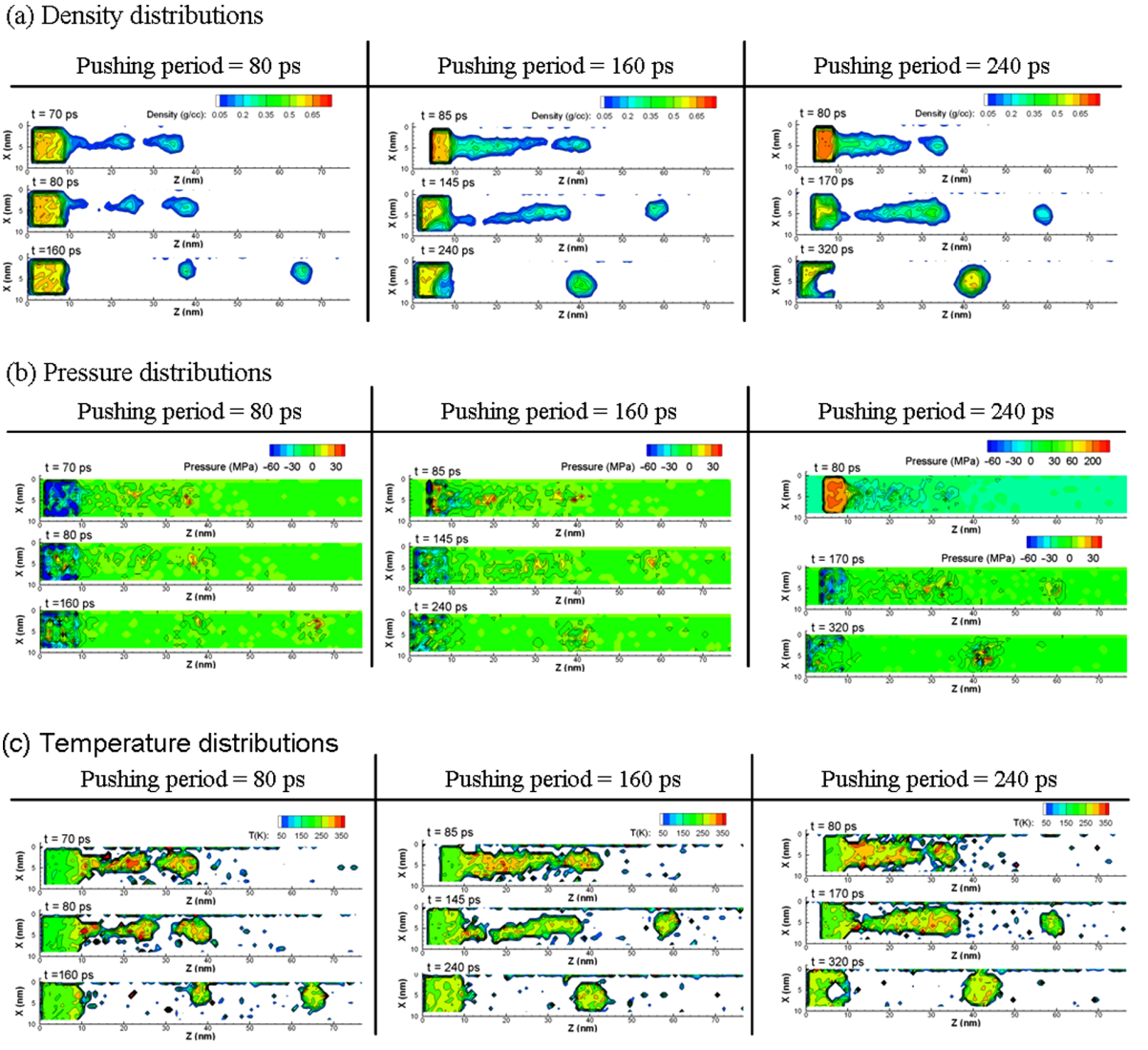

Figure 3. 2D plots of property distributions for various pushing periods.

reduces rapidly and finally tends to zero along the axis of the nozzle outlet. During the fall step, a negative pressure region appears at the reservoir wall. These results suggest a mechanism wherein the pressure port compresses the fluid molecules and forms high-pressure regions during the rise step. And during the fall step, fluid is drawn back into the reservoir by the force of attraction of the negative pressure regions inside the reservoir.

The temperature distributions are shown in Figure 3(c). We can observe that high-temperature regions appear in the contracting part of the nozzle channel during the rise step. It is obvious that shear-heating phenomena occurred along the region of contact. As a result of heat conduction and convection, the temperature distribution becomes uniform as the ejection process progresses. Subsequent to liquid ejection, we note that the temperature at the centre of the liquid thread is higher than that at the surface.

3.3 Thermal properties and sizes of droplet for various pushing periods

Figure 4 shows the number of ejected atoms at various pushing periods. We observe that the number of ejected atoms increases during the rise step in all the cases, and the number slightly decreases when the fall step starts. This shows that some molecules are drawn back into the reservoir as a result of the interaction with the plate during the fall step. Furthermore, the final results show that more atoms are ejected with an increase in the pushing period. The temperature changes for various pushing periods are shown in Figure 5. We observe that the temperature increases with time during the rise step. It is obvious that shear-heating phenomena occur when the liquid flows through the nozzle channel. Furthermore, the plate compresses results in work done to the system. Thus, the case with the longest pushing period (240 ps) can attach to higher temperature than the others. Subsequent to the rise step, the temperature steeply decreases because the plate does a negative work as it moves in the reverse direction. Subsequent to the fall step, the temperature remains constant, and the final temperature increases with the pushing period. Figure 6 shows the evolution of pressure inside the reservoir for various pushing periods. We observe that the pressure decreases as molecules are ejected from the nozzle during the rise step. Furthermore, the pressure reduces rapidly and finally tends to zero during the fall step. This is because a vacuum environment surrounds the nozzle system.

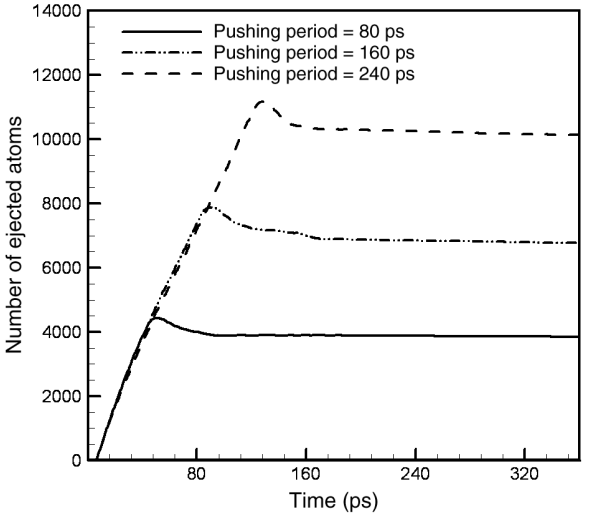

Figure 4. Number of ejected atoms for various pushing periods.

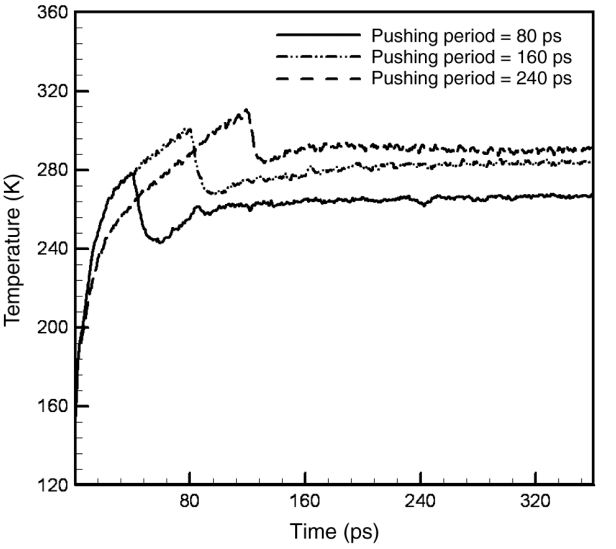

Figure 5. Temperature changes observed for various pushing periods.

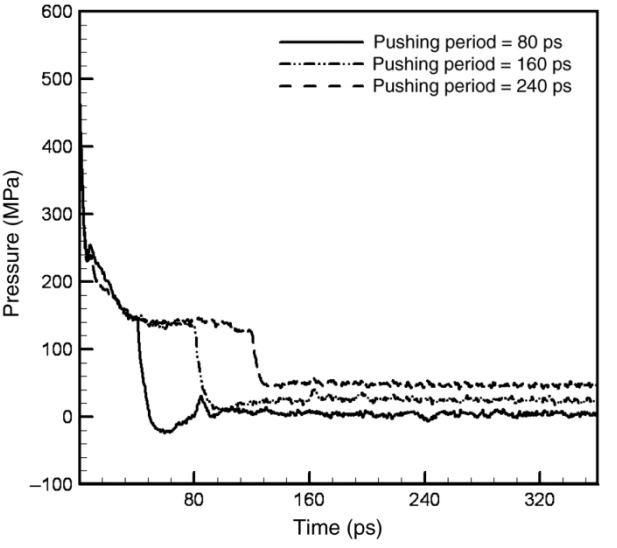

Figure 6. Evolution of reservoir pressure for various pushing periods.

Figure 7 shows the energy evolution of the ejection processes for various pushing periods; this figure is used to gain insights into the mechanism of the nanoejection process. The total energy includes both kinetic energy and Lennard-Jones potential energy. Investigation of the energy terms for various ejection processes shows that they increase with time during the rise step; the energy terms do not display any obvious change during the fall step. Subsequent to the rise step, the kinetic energy decreases rapidly in all cases. This is because the plate moves backwards and draws back the fluid molecules. As a result, the different steps involved in the ejection process influence the energy terms. For cases with higher pushing periods, the energy profiles can attach the higher value. This is because the fluid molecules obtain more kinetic energy with an increase in the plate compression time. As a result, for cases with higher pushing periods, the energy terms show an increase greater than that observed for the other cases. In contrast, for cases with the lowest pushing period, the evolution of energy profiles are similar to that observed in the other cases but attached to a lower energy level.

The droplet diameter for various pushing periods is shown in Figure 8. Various symbols represent the droplet diameters along the *x*-, *y*- and *z*-axes. To avoid the effect of initial conditions, the values are obtained from three simulations with different initial conditions. The results show that the size of the droplets is linearly dependent on the pushing period. The results suggest that piezoelectric nanoejection can create droplets of a specific size. We also observe that there are discrepancies in the diameters and directions of each droplet formed (Figure 8), which implies that the droplet is not spherical in such cases. This is because the diameter of the droplet is about 3–8 nm, and

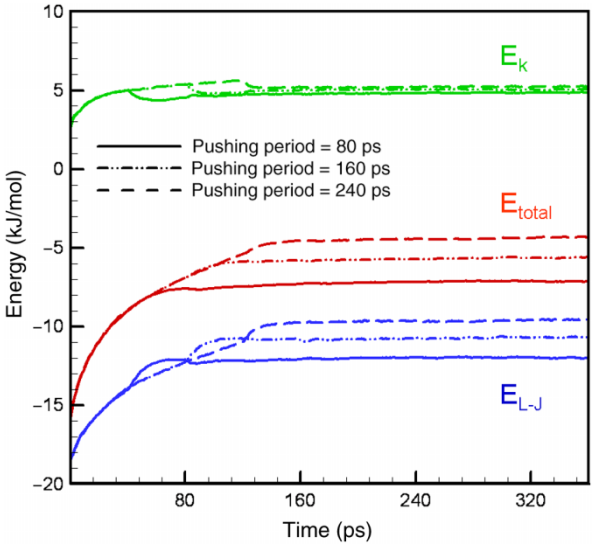

Figure 7. Results for the time evolution of the energy change for various pushing periods.

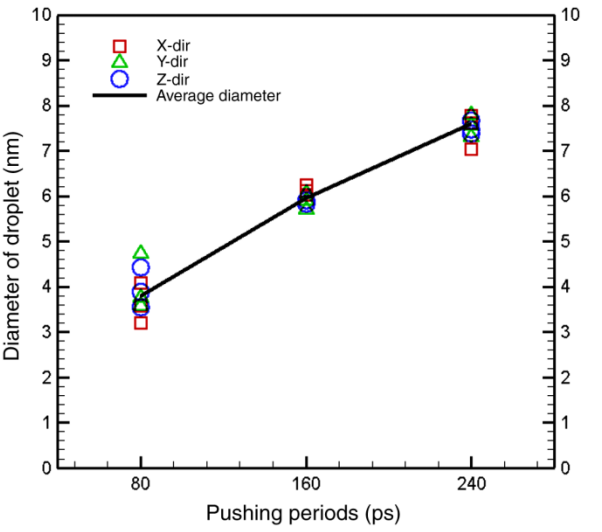

Figure 8. Droplet diameter for various pushing periods.

there are too few fluid molecules to form a perfect spherical structure. Furthermore, since the number of molecules in the low pausing period case is less, the discrepancy is more obvious than in the other cases.

3.4 The hydrodynamics equations of the breakup profiles for ejection process

In particular, the nonlinear dynamics and breakup of free-surface flows are usually described by the lubrication equation [5] (LE) which contains Equations (3) and (4). Equation (3) describes the velocity, $v(z,t)$; and Equation (4) describes the liquid thread radius, $h(z,t)$:

$$\partial_t v + v\partial_z v = -\frac{\gamma}{\rho}\partial_z \kappa + 3\frac{\eta}{\rho}\frac{\partial_z\left(h^2\partial_z v\right)}{h^2}, \tag{3}$$

$$\partial_t h + v\partial_z h = \frac{-(\partial_z v)h}{2}, \tag{4}$$

where γ represents the surface free energy of the fluid; η, the viscosity; ρ, the density; and the mean curvature κ is

$$\kappa(z,t) = \frac{1}{(h(z,t)\{[\partial_z h(z,t)]^2 + 1\}^{1/2})} - \frac{\partial_z^2 h(z,t)}{(1+[\partial_z h(z,t)]^2)^{3/2}}. \tag{5}$$

The LE based on the Navier–Stokes equation shows that the repetition of forming self-similar long thread structures would continue until it was interrupted by breakup. However, influences of thermal fluctuations change the dynamic process and jet structures in the nanoscale. Thus, to describe the dynamic of nanojets, we should include the influences of thermal fluctuations.

The SLE [7,8], where a size-dependent stress fluctuation (standard Gaussian white noise, N) is included, is demonstrated for comparison with the MD simulation results [7]. Therefore, functions (3) and (4) will be modified to Equations (6) and (7),

$$\partial_t v + v\partial_z v = -\frac{\gamma}{\rho}\partial_z \kappa + 3\frac{\eta}{\rho}\frac{\partial_z(h^2\partial_z v)}{h^2} - \frac{1}{\rho}\sqrt{\frac{6k_B T\eta}{\pi}}\frac{\partial_z(hN)}{h^2}, \quad (6)$$

$$\partial_t h + v\partial_z h = \frac{-(\partial_z v)h}{2}. \quad (7)$$

Figure 9(a) shows the breakup profiles calculated from the LEs and SLEs. We can find that the breakup structure in the LE exhibits an extended thin, long thread. The breakup structure in the SLE shows that the liquid thread resembles two cones and leads to a symmetric pinch-off. The MD simulation results with the longest pushing period (240 ps) are shown in Figure 9(b). The first and the second breakup profiles appear in the 70 and 160 ps, respectively. We can find that the first breakup profile is similar to the results of the SLE. The double-cone structures appear in those breakup profiles. These results show that the breakup profiles obey the SLE equation in the nanoscale.

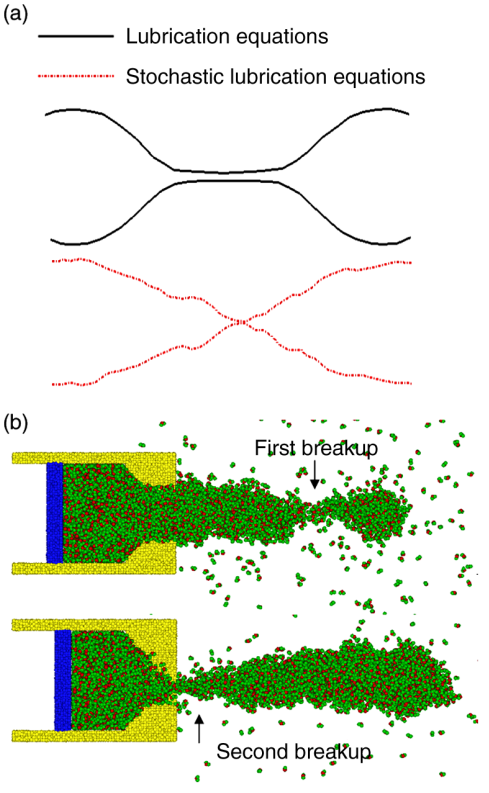

Figure 9. Breakup profiles of (a) breakup profiles calculated from the LEs and SLEs and (b) the results from MD simulation in the case of the 240 ps pushing period.

Figure 10 shows the time dependence of the minimum radius, R_{min}. The results are gathered from the first and second breakup with the longest pushing period (240 ps). The results show that the behaviours of the neck profiles obey $R_{min} \propto (t_0 - t)^{\alpha}$, where the t_0 is the pinch-off time. The SLE analysis and MD results suggest that the value of α is 0.418 [7]; and the macroscopic results show that the value of α is about 1 [8]. From Figure 10, the power exponent of the fitting curve of the first breakup is 0.566 and the second breakup is 0.903. The results show that the first breakup is similar to the related research results [7]; and the second breakup is influenced by the intra-force and the drag force exerted by the plate. Therefore, the second breakup will tend to decay fast and lead to a long tail structure.

4. Conclusion

Non-equilibrium MD is used in this study to simulate piezoelectric nanoejection processes at various pushing periods. Based on the simulation, discussions and some results of these simulations are presented in this paper. Two different breakups under different mechanisms are found in this study. The first one is the double-cone structure, which is a result of the balance between surface tension and inertia force; the second one is the long tail structure, which is a result of the intra-force and the drag force exerted by the plate. The property distribution contours show that density and pressure are neither uniform nor continuous at the nanoscale during the ejection process. Local high-pressure regions appear near the pressure port during the rise step, and a negative pressure region appears at the reservoir wall during the

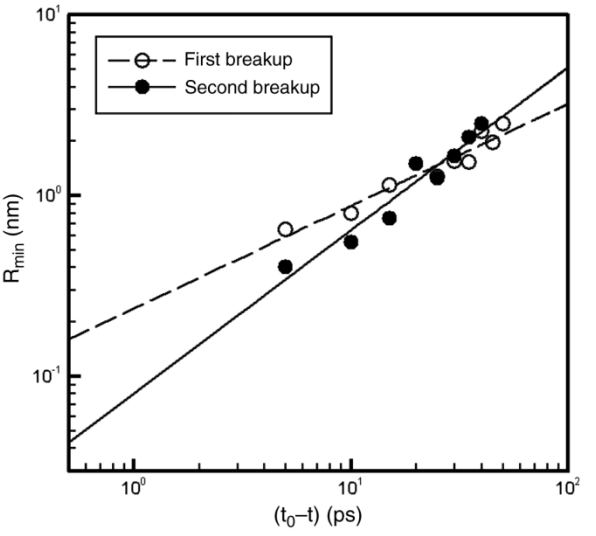

Figure 10. Time dependence of the minimum radius, R_{min}, in the case of the longest pushing period (240 ps).

fall step. As the plate compresses, shear-heating phenomena occur in the region of contact with the nozzle channel during the rise step. The evolutions of thermal properties show that the number of ejected atoms, system temperature and energy increase with time during the rise step, and these parameters slightly decrease during the fall step. The reservoir pressure decreases during the rise step and reduces rapidly during the fall step. A linear relationship between the size of the droplets and the pushing periods is observed in this study. The hydrodynamics equations (LE and SLE) of the breakup profiles are discussed to compare with the MD simulation results. The results show that piezoelectric nanoejection processes can provide control over the size of droplets and may possibly have many technological applications.

Acknowledgements

The authors thank the National Science Council of the R.O.C. for partially supporting this research under Contract No. NSC 95-2221-E-007-082.

References

[1] R.G. Sweet, *High frequency recording with electrostatically deflected ink jets*, Rev. Sci. Instrum. 36 (1964), pp. 131–136.
[2] F. Korte, J. Koch, J. Serbin, A. Ovsianikov, and B.N. Chichkov, *Three-dimensional nanostructuring with femtosecond laser pulses*, IEEE T. Nanotech. 3 (2004), pp. 468–472.
[3] N. Naik, C. Courcimault, H. Hunter, J. Berg, J. Lee, K. Naeli, T. Wright, M. Allen, O. Brand, A. Glezer, and W. King, *Microfluidics for generation and characterization of liquid and gaseous micro- and nano-jets*, Sensor Actuator 134 (2007), pp. 119–127.
[4] M. Gad-el-Hak, *MEMS: Applications*, CRC Press, Boca Raton, FL, 2005.
[5] J. Eggers, *Nonlinear dynamics and breakup of free-surface flows*, Rev. Mod. Phys. 69 (1997), pp. 865–929.
[6] C. Wagner, Y. Amarouchene, D. Bonn, and J. Eggers, *Droplet detachment and satellite bead formation in viscoelastic fluids*, Phys. Rev. Lett. 95 (2005), pp. 164504-1–164504-4.
[7] M. Moseler and U. Landman, *Formation, stability, and break-up of nanojets*, Science 289 (2000), pp. 1165–1169.
[8] W. Kang and U. Landman, *Universality crossover of the pinch-off shape profiles of collapsing liquid nanobridges in vacuum and gaseous environments*, Phys. Rev. Lett. 98 (2007), pp. 064504-1–064504-4.
[9] H. Shin, M. Oschwald, M.M. Micci, and W. Yoon, *Influence of thermodynamic state on nanojet break-up*, Nanotechnology 16 (2005), pp. 2838–2845.
[10] Y.S. Choi, S.J. Kim, and M.-U. Kim, *Molecular dynamics of unstable motions and capillary instability in liquid nanojets*, Phys. Rev. E 73 (2006), pp. 016309-1–016309-6.
[11] K. Ichiki and S. Consta, *Disintegration mechanisms of charged aqueous nanodroplets studied by simulations and analytical models*, J. Phys. Chem. B 110 (2006), pp. 19168–19175.
[12] S. Murad and I.K. Puri, *Nanoscale jet collision and mixing dynamic*, Nano Lett. 7 (2007), pp. 707–712.
[13] H.-H. Shin, D. Suh, and W.-S. Yoon, *Non-equilibrium molecular dynamics of nanojet injection in a high pressure environment*, Microfluid. Nanofluid. 5 (2008), pp. 561–570.
[14] W. Kang, U. Landman, and A. Glezer, *Thermal bending of nanojets: Molecular dynamics simulations of an asymmetrically heated nozzle*, Appl. Phys. Lett. 93 (2008), pp. 123116-1–123116-3.
[15] J. Eggers, *Dynamics of liquid nanojets*, Phys. Rev. Lett. 89 (2002), pp. 084502-1–084502-4.
[16] A. Tiwari and J. Abraham, *Dissipative particle dynamics simulations of liquid nanojet breakup*, Microfluid. Nanofluid. 4 (2008), pp. 227–235.
[17] J.M. Haile, *Molecular Dynamics Simulation: Elementary Method*, John Wiley & Sons, New York, 1997.
[18] D.C. Rapaport, *The Art of Molecular Dynamics Simulation*, Cambridge University Press, Cambridge, 1995.
[19] D. Stauffer, *Annual Reviews of Computational Physics IX*, World Scientific Publishing Company, Singapore, 2001.
[20] S. Toxvaerd, *Molecular dynamics calculation of the equation of state of liquid propane*, J. Chem. Phys. 91 (1989), pp. 3716–3720.
[21] W.L. Jorgensen, J.D. Madura, and C.J. Swenson, *Optimized intermolecular potential functions for liquid hydrocarbons*, J. Am. Chem. Soc. 160 (1984), pp. 6638–6646.
[22] C.-F. Dai and R.-Y. Chang, *Molecular dynamics simulation of thread break-up and formation of droplets in nanoejection system*, Mol. Simul. 35 (2008), pp. 334–341.
[23] X.-J. Fan, P.-T. Nhan, N.T. Yong, and X. Diao, *Molecular dynamics simulation of a liquid in a complex nano channel flow*, Phys. Fluids 14 (2002), pp. 1146–1153.
[24] S. Nosé, *A unified formulation of the constant temperature molecular dynamics methods*, J. Chem. Phys. 81 (1984), pp. 511–519.
[25] K.A. Al-Matar, *A generating equation for mixing rules and two new mixing rules for interatomic potential energy parameters*, J. Comput. Chem. 25 (2004), pp. 660–668.